inorganics

MDPI

Article

Correlation of EPR and Photoluminescence Analysis for Crystalline Defects in Eu^{3+}/Yb^{3+}-Doped Lutetium Silicate Sol–Gel Powders

Andrea Danielle Cancino-Moreno [1,†], Arturo López-Marure [1,†], Stephany Natasha Arellano-Ahumada [2], Daniel Ramírez-Rosales [2,*] and Margarita García-Hernández [3,4,*]

[1] Instituto Politécnico Nacional, Centro de Investigación en Ciencia Aplicada y Tecnología Avanzada Unidad Altamira, Carretera Tampico-Puerto Industrial Altamira, Altamira Tamaulipas 89600, Mexico; acancinomo1800@alumno.ipn.mx (A.D.C.-M.); arlopezm@ipn.mx (A.L.-M.)
[2] Instituto Politécnico Nacional, Escuela Superior de Física y Matemáticas, Avenida Instituto Politécnico Nacional, San Pedro Zacatenco, San Pedro Zacatenco, Mexico City 07738, Mexico; torchynsnat@yahoo.com.mx
[3] Instituto Politécnico Nacional, CECyT 16 "Hidalgo", Carretera Pachuca Actopan Km 1+500, San Agustín Tlaxiaca 42162, Hidalgo, Mexico
[4] Instituto Politécnico Nacional, Unidad Profesional Interdisciplinaria de Ingeniería Campus Hidalgo, Carretera Pachuca Actopan Km 1+500, San Agustín Tlaxiaca 42162, Hidalgo, Mexico
* Correspondence: dramirezr@ipn.mx (D.R.-R.); margarciah@ipn.mx (M.G.-H.); Tel.: +52-5557296000 (ext. 55050 or 83902) (D.R.-R. & M.G.-H.)
† These authors contributed equally to this work.

Abstract

Crystalline defects such as oxygen vacancies have been studied little by electron paramagnetic resonance (EPR) spectroscopy for silicate-based luminescent materials. In this study, lutetium oxyorthosilicate powders were prepared by the sol–gel method, using TEOS (silicon source) and rare earth salts as precursors. The cross-linking agent, Glymo, contributed silicon atoms to the precursor solution in all systems. The addition of Glymo to Lu_2SiO_5, Lu_2SiO_5:Eu and Lu_2SiO_5:Eu/Yb influenced the morphology and chemical structure of the powders, leading to $Lu_2Si_2O_7$ formation. The crystalline defects in the lutetium silicate systems were investigated by EPR spectroscopy, and several defects related to oxygen were identified, as well as impurities from the precursors. Photoluminescence emission spectra revealed Eu^{3+} transitions between $^5D_0 \rightarrow {}^7F_0$, $^5D_0 \rightarrow {}^7F_1$ and $^5D_0 \rightarrow {}^7F_2$ under 258 nm excitation, in addition to oxygen vacancy emissions between 500 and 550 nm. Oxygen vacancies were identified and confirmed by correlating EPR and photoluminescence studies.

Keywords: lutetium silicate; glymo; oxygen vacancies; luminescence; EPR

check for updates

Academic Editors: Ivana Zekovic and Jovana Periša

Received: 22 September 2025
Revised: 17 October 2025
Accepted: 20 October 2025
Published: 22 October 2025

Citation: Cancino-Moreno, A.D.; López-Marure, A.; Arellano-Ahumada, S.N.; Ramírez-Rosales, D.; García-Hernández, M. Correlation of EPR and Photoluminescence Analysis for Crystalline Defects in Eu^{3+}/Yb^{3+}-Doped Lutetium Silicate Sol–Gel Powders. *Inorganics* **2025**, *13*, 343. https://doi.org/10.3390/inorganics13110343

Copyright: © 2025 by the authors. Licensee MDPI, Basel, Switzerland. This article is an open access article distributed under the terms and conditions of the Creative Commons Attribution (CC BY) license (https://creativecommons.org/licenses/by/4.0/).

1. Introduction

It is known that crystals have defects in their crystalline structure. Oxygen vacancies (V_O) are an example of this type of defect. The experimental characterization of V_O has been conducted using X-ray photoelectron spectroscopy (XPS), Raman spectroscopy complemented by UV–Vis spectroscopy [1–3] and EPR spectroscopy, primarily for other applications such as photocatalytic activity [4]. In structural studies related to crystalline defects in silicate-based luminescent materials, little has been studied by correlating EPR spectroscopy and photoluminescence (PL) [5,6]. Previous studies have experimentally and theoretically shown the presence of oxygen vacancies in lutetium silicate systems doped with Ce^{3+} [7,8]. Lutetium oxyorthosilicate is a rare earth silicate with similar characteristics

to commercial phosphors, such as high density (7.4 g/cm^3), and for scintillation application, a high light output yield (~27,500 photons/MeV), and a fast response (~40 ns), enabling the system to be able to be doped with different rare earth ions [9–14]. Structurally, the fundamental silicate unit consists of a $[SiO_4]^{4-}$ tetrahedron; the Si-O bond tends to be of a more covalent character than ionic, resulting in a stable bond [15]. The moderate repulsive forces between silicon atoms allow the linking of $[SiO_4]^{4-}$ via common oxygen atoms to form many polymorphs; thus, silicate can be organized in different ways, like tetrahedron rings, chains, sheets or isolated. Generally, silicate compounds contain Si–O–M bonds, where the M–O bond is weaker than the Si–O bond due to the metal ions having a lower valence than silicon. This results in the formation of $[SiO_4]^{4-}$ tetrahedra where silicon attracts oxygen ions more strongly than the metal ions [15]. Rare earth silicate compounds consist of isolated (SiO_4) tetrahedra or groups of (Si_2O_7) and (Si_3O_{10}), where the rare earth cations are coordinated from six to ten oxygen atoms. The binary system RE_2O_3–SiO_2 with a composition of 1:1 has two different monoclinic structural types with the space group $P2_1/c$ for type A and the space group C2/c for type B. In rare earth (RE) silicates, the RE–O bond is essentially electrostatic because of the strongly electropositive nature of RE^{3+}. Lu_2SiO_5 is an oxyorthosilicate compound containing two types of anions: the (SiO_4) tetrahedra and non-silicon-bonded oxygen ions. Lutetium oxyorthosilicate crystallizes in a monoclinic structure containing two crystallographic sites for lutetium in the space group C2/c (type B) [16]. The first lutetium site (Lu1) is coordinated with six oxygen atoms with Lu–O bond distances in the range of 2.13–2.25 Å, and the second lutetium site (Lu2) is coordinated with seven oxygen atoms with Lu–O bond distances in the range of 2.12–2.62 Å [17]. The aim of this investigation is to identify the crystalline defects present in lutetium silicate phosphors. This will contribute to the structural analysis of luminescent materials by considering intrinsic defects and correlating EPR spectroscopy analysis with photoluminescence properties.

2. Results and Discussions

The XRD patterns of the $Lu_2Si_2O_7/Lu_2SiO_5$/Glymo (LSG), $Lu_2Si_2O_7/Lu_2SiO_5$/Glymo:Eu^{3+} (LSG:Eu) and $Lu_2Si_2O_7/Lu_2SiO_5$/Glymo:Eu^{3+}/Yb^{3+} (LSG:Eu/Yb) powders calcined at 1100 °C are shown in Figure 1A. The stable phase (type B) of Lu_2SiO_5 with a monoclinic structure and space group C2/c (ICSD 98-008-9624) was identified in all samples. Type B $Lu_2Si_2O_7$ (ICSD 98-041-2249) was also present due to the addition of Glymo as the cross-linking agent, which acts as a silicon precursor like TEOS, contributing silicon atoms to the reaction. To obtain the $Lu_2Si_2O_7$ system by the Sol–Gel method, it is necessary to use 1 mol of Lu_2O_3 sol and 2 mol of SiO_2 sol. Even if only 1 mol of SiO_2 sol was used, the amount of Glymo added to the precursor solution contributes 1 mol of silicon to form lutetium pyrosilicate ($Lu_2Si_2O_7$).

The hydrolyzable methoxy groups in Glymo can undergo nucleophilic attack by the solvents present in the lutetium silicate precursor solution, such as ethanol and water, where the OH^- groups displace a hydrogen atom from the methoxy group to interact with the lutetium atoms. In this way, Glymo contributes a larger amount of silicon atoms, thus forming $Lu_2Si_2O_7$. The crystallographic planes were identified for the main crystalline signals of Lu_2SiO_5 (denoted with "*") and $Lu_2Si_2O_7$ (denoted with "•"). As demonstrated in the diffractogram, a greater number of signals match for lutetium pyrosilicate ICSD no. 98-041-2249, thus indicating that the addition of Glymo favored the formation of $Lu_2Si_2O_7$ and as a secondary phase, lutetium oxyorthosilicate. The crystallographic signals for the three samples were identified at the same diffraction angles, indicating no displacement, which suggests the incorporation of Eu^{3+} and Yb^{3+} as substitute atoms replacing the Lu site in the crystalline structure. The average crystallite size was calculated using Scherrer's

formula $D = k\lambda/\beta\cos\theta$ [18], where D is the average crystallite size, k is the shape factor, λ is the X-ray wavelength, β is the peak width at FWHM and θ is the Bragg angle at 16, 22 and 19 nm for the LSG, LSG:Eu and LSG:Eu/Yb samples, respectively.

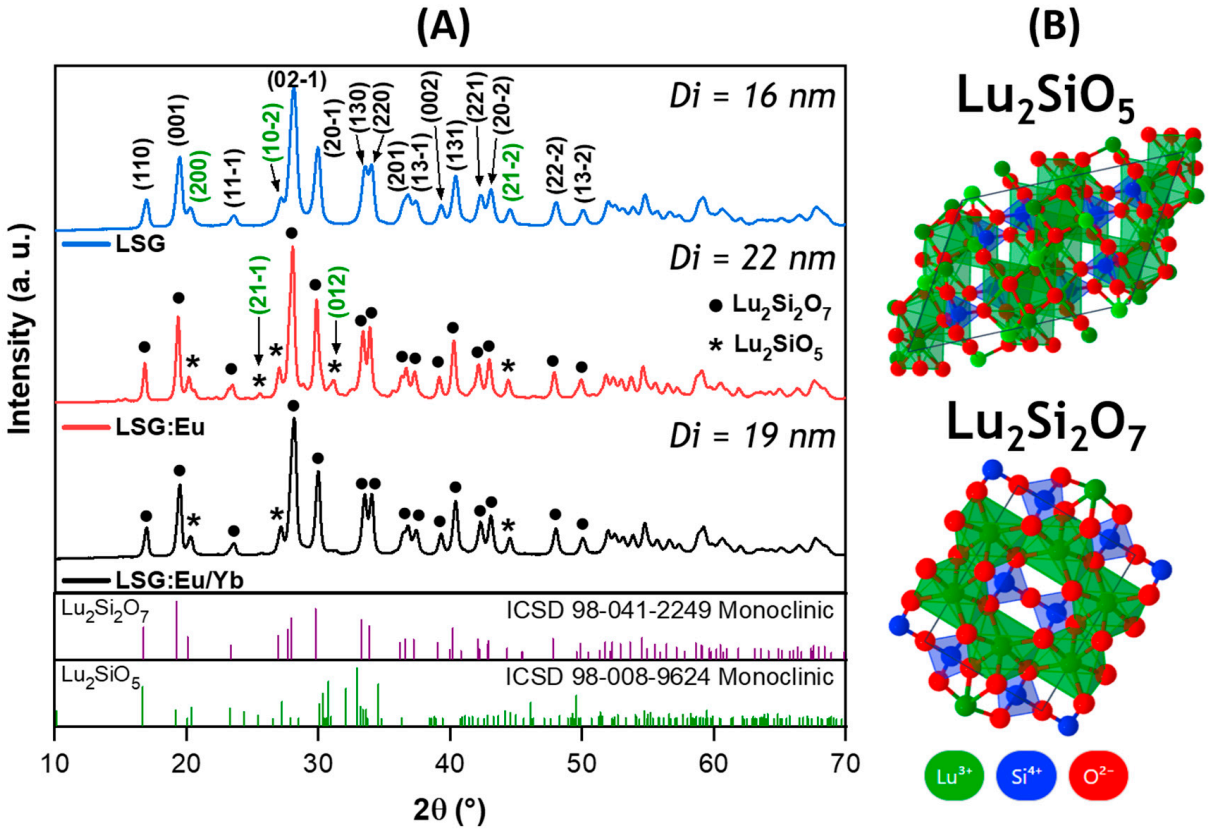


Figure 1. X-ray diffraction patterns for (**A**) lutetium silicate systems (LSG, LSG:Eu and LSG:Eu/Yb) obtained by Sol–Gel method and calcined at 1100 °C for 2 h, where Di is the average crystallite size, [•] indicates the $Lu_2Si_2O_7$ phase, [*] indicates the Lu_2SiO_5 phase and (**B**) shows Lu_2SiO_5 B type and $Lu_2Si_2O_7$ B type monoclinic structures.

Porosity was evident in Figure 2 due to the elimination of vapors, forming cavities or empty spaces within the matrix. Initially, the addition of Glymo favored the interactions with the precursor solution, increasing the formation of a 3D network during the Sol–Gel process because of the ability of Glymo molecules to cross-link [19,20]. Subsequently, the heat treatments eliminated the organic Glymo components, generating the observed porosity. The larger surface area, attributed to porosity, facilitates interaction with the environment; for example, it enables oxygen loss during heat treatments. Defects have been observed on surfaces, where they concentrate and stabilize, thus forming oxygen vacancies in the system [21–23].

Figure 3 shows the EPR spectra for the lutetium silicate powders with the addition of Glymo. For each sample (LSG, LSG:Eu and LSG:Eu/Yb), a very broad signal appears to extend from 0 to 600 mT or more and increases its intensity in relation to the amount of lanthanide ions; the signal width is due to the short relaxation time that these ions have [24]. Also, these signals present a maximum at approximately g~16.344 (40 mT). This is important because it allows us to infer the possible oxidation states for the rare earth ions. For Lu ($[Xe]4f^{14}5d^{1}6s^{2}$), the common oxidation state is 3+, and although less frequent, it can be 2+, 1+ and 0. For EPR signals to exist, there must be at least one unpaired electron; this implies that the EPR signals due to lutetium could originate from some Lu^{2+} ions present in the samples, since the other oxidation states do not provide unpaired electrons that could

contribute to the EPR signal. The radii of Lu^{2+} are considerably smaller than that of Lu^{3+} because the loss of electrons, particularly from the 6s orbitals, results in greater nuclear attraction for the remaining electrons and a reduction in the size of the ion. From the above, it can be deduced that the possible existence of Lu^{2+} ions and the decrease in their atomic radius with respect to Lu^{3+} would break the crystallinity of the lattice, creating defects or vacancies, which were detected by EPR around g~2 (H~333 mT), as shown in Figure 3.

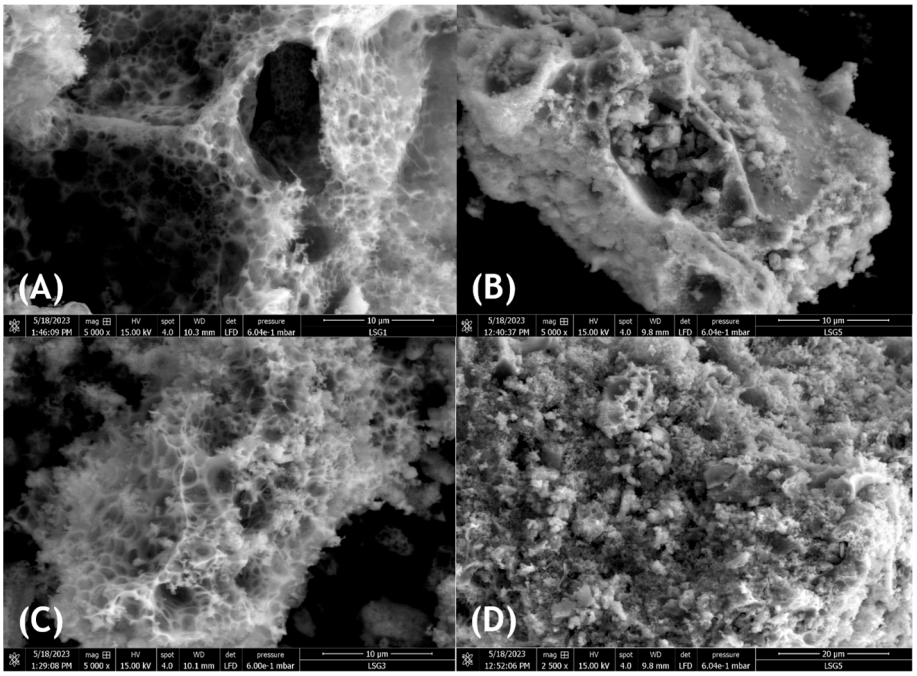


Figure 2. SEM images of (**A**) $Lu_2Si_2O_7/Lu_2SiO_5$/Glymo (LSG), (**B**) $Lu_2Si_2O_7/Lu_2SiO_5$/Glymo:Eu^{3+} (LSG:Eu) and (**C**), (**D**) $Lu_2Si_2O_7/Lu_2SiO_5$/Glymo:Eu^{3+}/Yb^{3+} (LSG:Eu/Yb) powders obtained by Sol–Gel method calcined at 1100 °C for 2 h.

For europium ([Xe]$4f^7 6s^2$), the most common oxidation state is 3+; but it is also common to find the 2+ state in a stable manner [25]. However, Eu^{3+} is not paramagnetic, implying that there may also be a certain amount of Eu^{2+} ions that could contribute to the increased EPR signal intensity. As shown in Figure 3, the signal intensity at g~16.344 (40 mT) for LSG and LSG:Eu is not significant, implying that the oxidation state of Eu is 3+. Nevertheless, the appearance of new vacancies or defects is evident by EPR, as can be seen in the g~2 region (H~333 mT). This indicates that Eu entered the lattice substitutionally, and due to the different atomic radii of the Lu^{2+} and Eu^{3+} ions, a greater detriment in the lattice crystallinity of the LSG:Eu sample is induced compared to LSG. Analogous to Eu, ytterbium ([Xe]$4f^{14} 6s^2$) also exhibits stable oxidation states 3+ and 2+; however, the only oxidation state detectable by EPR is 3+. Two related effects are observed in the EPR spectrum (Figure 3) for the LSG:Eu/Yb sample: the first effect is the increase in signal intensity at g ~ 16.344; while the second is the significant reduction in defects (signals at g~2). This implies that Yb enters the lattice substitutionally, most likely at Eu ion sites with oxidation states of 3+, which increases the intensity and crystallinity of the g~16 signal by significantly reducing the defects in the lattice as observed in the g~2 region. Around 158 mT, an absorption signal is identified with a value of g~4.25, which is related to impurities of Fe^{3+} ions present in the precursors [26]. Such impurity of Fe^{3+} in EPR analysis is of little importance in the discussion of defects or vacancies.

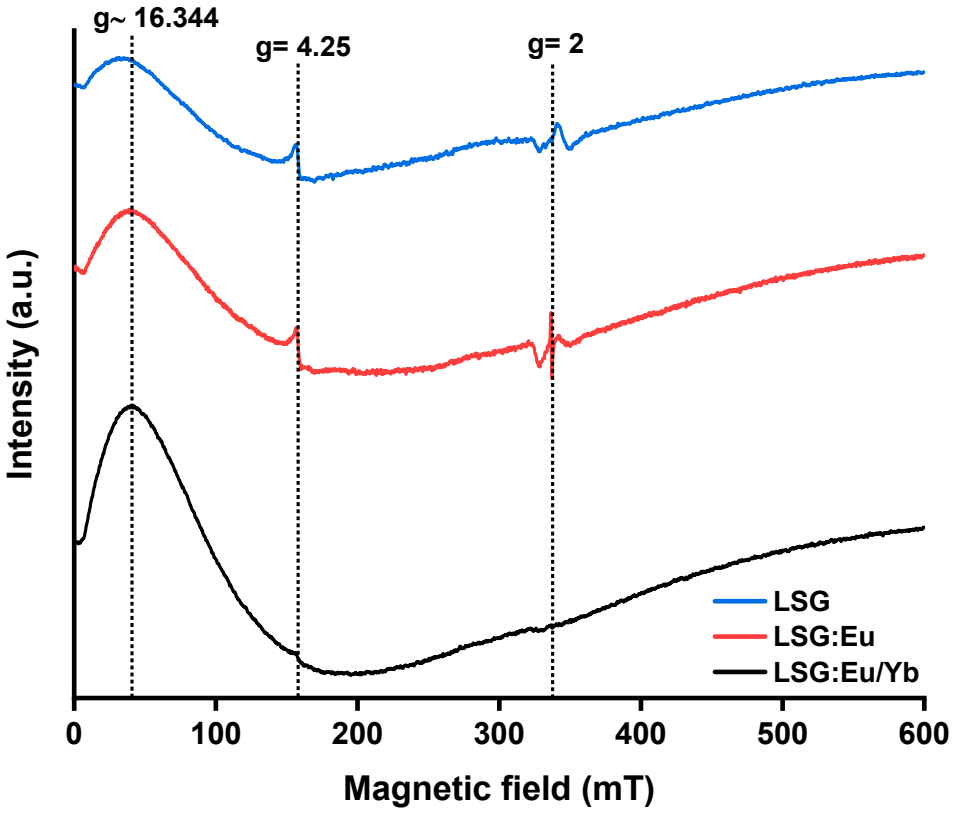


Figure 3. EPR spectra obtained at 77 K with X-band (~9.5 GHz) for $Lu_2Si_2O_7/Lu_2SiO_5$/Glymo (LSG), $Lu_2Si_2O_7/Lu_2SiO_5$/Glymo:Eu^{3+} (LSG:Eu) and $Lu_2Si_2O_7/Lu_2SiO_5$/Glymo:Eu^{3+}/Yb^{3+} (LSG:Eu/Yb) powders obtained by Sol–Gel method and calcined at 1100 °C for 2 h.

In the 300 to 400 mT range, oxygen-related absorption signals are identified. All samples were calcined at 1100 °C for 2 h and then irradiated at 258 nm for photoluminescence measurements. Lutetium silicate is a ceramic material that has a theoretical bandgap of 4.68 eV [27]. The excitation source energy supplied to the system was 4.8 eV, which can promote the passage of electrons from the valence band to the conduction band, thus forming electron–hole pairs. The charge carriers generated can stabilize at defect sites, forming paramagnetic species detectable by EPR, as observed in the spectrum. On the other hand, the holes generated by exposure to ultraviolet light are stabilized at O^{2-} sites mainly on the sample surface, forming O^- ions. All samples show intense EPR signals in the region of g = 2 (Figures 3 and 4), which is typical for free radicals and paramagnetic structural defects.

Figure 4 shows the absorption signals related to defects assigned to oxygen. From the three lutetium silicate systems (LSG, LSG:Eu and LSG:Eu/Yb), signal B is identified, and it is of anisotropic-axial type spectrum with values of g// = 2.021 and g⊥ = 2.002. This signal is found in different proportions due to the formation of holes in the system. That is, all the samples have a different concentration of defects, with the LSG:Eu sample being the one with the highest concentration of O^- type species, in addition to the A signal, which is isotropic and corresponds to an F^+ color center where an electron is trapped in an oxygen vacancy [28]. Previous studies reported that the signal corresponding to ionized oxygen vacancies (V'_O) is obtained in an interval with g values between 1.9560 and 2.0030 [29], obtaining in this case signal A with a value of g = 2.0014. On the other hand, sample LSG:Eu/Yb is the one with the lowest concentration of defects, with a relative amount of O^- type species of 1:2.5:4.8 for samples LSG:Eu/Yb:LSG:LSG:Eu, respectively.

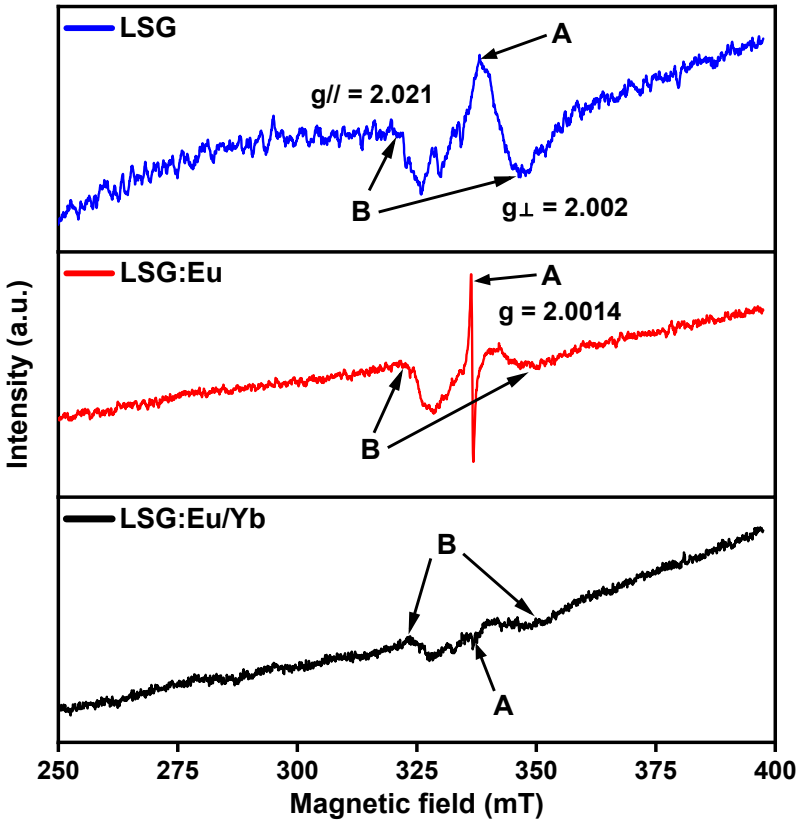


Figure 4. EPR spectra obtained at 77 K with X-band (~9.5 GHz) from 250 to 400 mT corresponding to defects assigned to oxygen for $Lu_2Si_2O_7/Lu_2SiO_5$/Glymo (LSG), $Lu_2Si_2O_7/Lu_2SiO_5$/Glymo:Eu^{3+} (LSG:Eu) and $Lu_2Si_2O_7/Lu_2SiO_5$/Glymo:Eu^{3+}/Yb^{3+} (LSG:Eu/Yb) powders obtained by Sol–Gel method and calcined at 1100 °C for 2 h.

The excitation spectra for lutetium silicate systems are shown in Figure 5A when monitored at 612 nm, which corresponds to the characteristic emission ($^5D_0 \rightarrow {}^7F_2$) of Eu^{3+} ion. Absorption signals related to Eu^{3+} ion are identified at 360, 380, 391, 400 and 413 nm which are attributed to $^5D_4 \leftarrow {}^7F_0$, $^5L_7 \leftarrow {}^7F_0$, $^5L_6 \leftarrow {}^7F_0$, $^5L_6 \leftarrow {}^7F_1$ and $^5D_3 \leftarrow {}^7F_1$ respectively [23,30]. Defects like oxygen vacancies can absorb excitation energy, giving rise to absorption bands different to the dopant ion in the excitation spectrum, and thus the absorption signals at 298 and 320 nm are attributed to defects [31,32]. The charge transfer band (CTB) between the oxygen to europium ions (O-Eu) is identified as a broad absorption signal centered at ~250 nm. The emission spectra for the three lutetium silicate samples (LSG, LSG:Eu and LSG:Eu/Yb) in Figure 5B were obtained at an excitation wavelength of 258 nm. It has been reported that defects can introduce energy levels for electrons in the bandgap of the material [33]. As observed in the EPR spectra, all samples exhibit defects associated with O^-, like oxygen vacancies.

The electrons that are not trapped by intrinsic defects in the system recombine with the photogenerated holes in the valence band. The excitation wavelength used for the measurement corresponds to the charge transfer band between the O–Eu (λ_{exc} = 258 nm), and emissions related to oxygen vacancies at approximately 513 and 540 nm were observed for all the systems [34,35]. Previous studies have discussed the role of oxygen vacancies, which can act as intrinsic luminescent centers [36], and are also able to function as sensitizers, thereby transferring energy to activators [37]. It is possible that an energy transfer occurs between oxygen vacancies and Eu^{3+} ions, as absorption signals associated with oxygen vacancies were identified in the excitation spectra. In the case of LSG:Eu and LSG:Eu/Yb, several emissions corresponding to Eu^{3+} ions were identified. The presence of

a $^5D_0 \rightarrow {}^7F_0$ transition (λ_{em} = 581 nm) indicates that the Eu^{3+} ion is inserted into the same crystallographic site for the $Lu_2Si_2O_7$ system. Since this transition ($^5D_0 \rightarrow {}^7F_0$) is known as a forbidden transition according to the selection rules, its observation is related to the J-mixing, where it can be assumed that a strong crystal-field effect occurs [38–40]. The emissions located at 588, 590 and 599 nm correspond to a magnetic dipole type transition ($^5D_0 \rightarrow {}^7F_1$) that is independent of the chemical environment surrounding the dopant ions; in this case, europium, unlike the emissions at 612 and 620 nm which correspond to an electric dipole type transition that is sensitive to the chemical environment surrounding the europium ion. It is important to mention that the characteristic emission of the europium ion is usually the one with the highest intensity corresponding to the electric dipole type ($^5D_0 \rightarrow {}^7F_2$); however as mentioned above, this transition is sensitive to the chemical environment, which is modified by adding Glymo as cross-linking agent, thus limiting the radiative transitions between the $^5D_0$ excited state and the $^7F_2$ ground state.

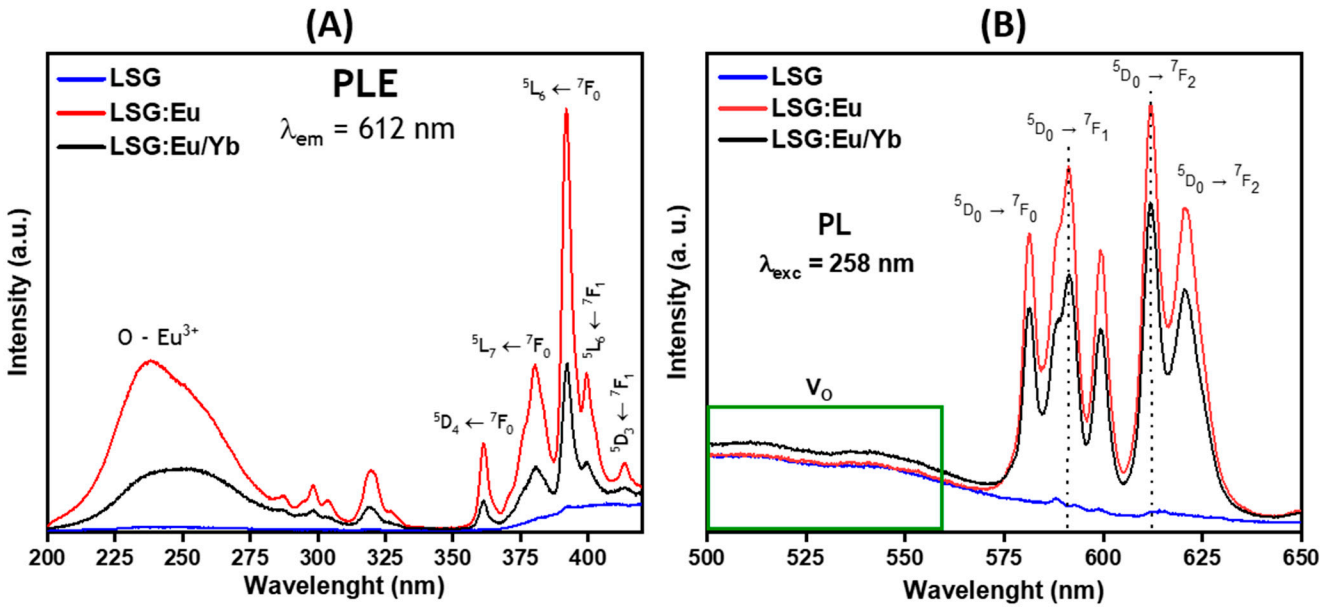


Figure 5. (**A**) Excitation spectra obtained when monitored at 612 nm and (**B**) PL emission spectra obtained at an excitation wavelength of 258 nm of $Lu_2Si_2O_7/Lu_2SiO_5$/Glymo (LSG), $Lu_2Si_2O_7/Lu_2SiO_5$/Glymo:Eu^{3+} (LSG:Eu) and $Lu_2Si_2O_7/Lu_2SiO_5$/Glymo:Eu^{3+}/Yb^{3+} (LSG:Eu/Yb) systems.

This may benefit the magnetic dipole type transition ($^5D_0 \rightarrow {}^7F_1$), so it is possible that the modification of the chemical environment, in addition to the generation of holes due to the excitation energy of the system, favor the effective radiative transitions between the $^5D_0$ excited state and the $^7F_1$ ground state, considering that there is no influence from the addition of Glymo on the emission at 590 nm [41]. The decrease in luminescence intensity in the LSG:Eu/Yb system can be attributed to the incorporation of the Yb^{3+} ion. The co-doping of the system with Yb^{3+} results in a competitive environment amongst the dopant ions, leading to the occupation of the preferential Lu site in the Lu_2SiO_5 phase, which is coordinated with seven oxygen atoms [17]. A schematic representation of the luminescence process is shown in Figure 6A. Electrons are excited from the valence band to the conduction band by the CTB (λ_{exc} = 258 nm), and the excited electrons in the conduction band have two possible paths: (1) De-excitation through non-radiative transitions to the level introduced by V_O, followed by emission (radiative transitions) at 513 and 540 nm. (2) Electrons decay to Eu^{3+} levels and through non-radiative relaxation to the bottom of the excited states ($^5D_0$), to decay by radiative transitions to the ground states ^7F_J (J = 0,

1, 2) while emitting at different wavelengths. Figure 6B corresponds to the chromaticity diagram obtained using the CIE 1931 standard which provides a visual understanding of color properties. The color coordinates for the LSG system are (0.3049, 0.6450), and this corresponds to the pure system which indicates only the oxygen vacancy emissions in the green region of the visible spectrum. For LSG:Eu and LSG:Eu/Yb systems, the color coordinates are (0.5345, 0.4518) and (0.5006, 0.4804), respectively, which are in the orange–red region of the diagram, and are typical of emissions for Eu^{3+} ions with similar intensities at $^5D_0 \rightarrow {}^7F_1$ and $^5D_0 \rightarrow {}^7F_2$ transitions. In summary, all lutetium silicate samples are active under irradiation and generate excitons which can stabilize in the intrinsic defects of the material. As observed in the SEM results (Figure 2), the porous morphology favors environmental interaction during heat treatments, generating intrinsic defects, such as oxygen vacancies, which were identified by EPR spectroscopy and correlated with the luminescent properties for the lutetium silicate systems. The presence of O^- type defects creates new energy levels in the bandgap of lutetium silicate, and the electrons that are stabilized in an oxygen vacancy form the color center.

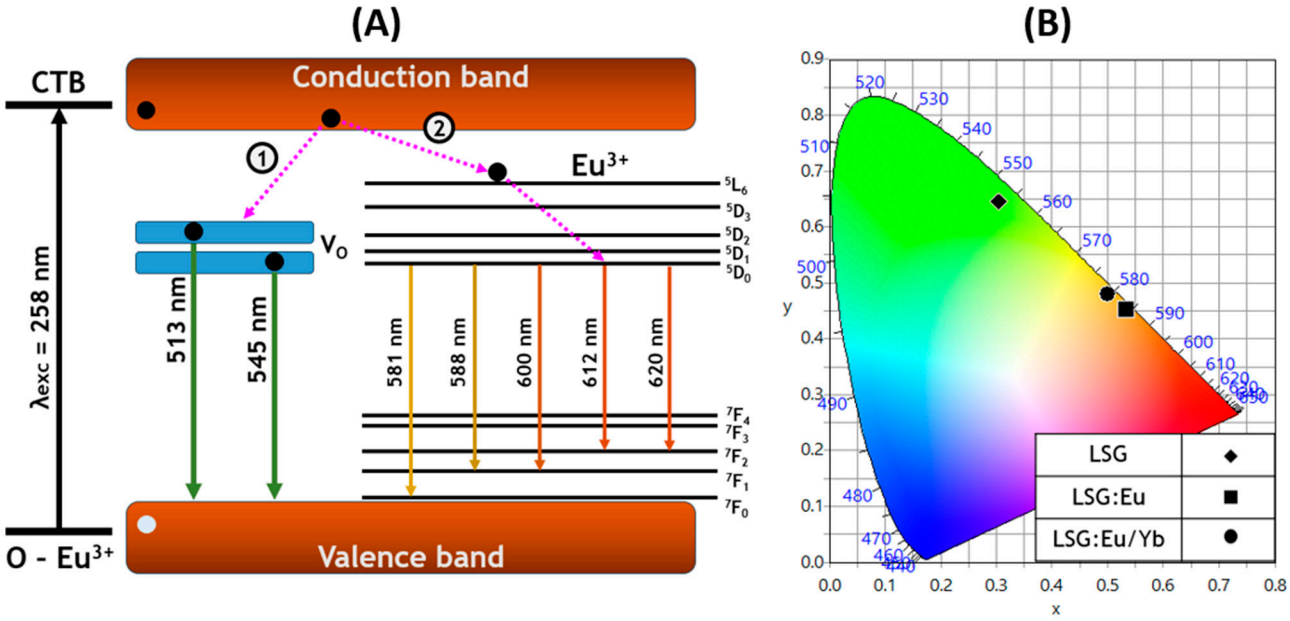


Figure 6. (**A**) Schematic representation of the luminescence process. Electrons (black circle), holes (white circle), radiative transition (solid line), non-radiative transition (dotted line) and pathways (circled numbers 1 and 2). (**B**) Chromaticity diagram of lutetium silicate systems.

3. Materials and Methods

3.1. Preparation of Powders

Lutetium nitrate [$Lu(NO_3)_3$, 99.9%], tetraethyl orthosilicate [TEOS $Si(OC_2H_5)_4$, 99%], europium nitrate [$Eu(NO_3)_3$, 99.9%], ytterbium chloride [$YbCl_3$, 99.9%], ethanol [C_2H_5OH, 99%], acetylacetone [AcAc $C_5H_8O_2$, 99%] and glycidyloxypropyl trimethoxysilane [Glymo $C_9H_{20}O_5Si$, 98%] were used as the starting materials. The lutetium silicate powders were obtained by the Sol–Gel method. Firstly, $Lu(NO_3)_3$ was mixed with ethanol and the chelating agent AcAc in a 1:1 molar ratio of Lu:AcAc under vigorous stirring for an hour to obtain the Lu_2O_3 sol [42–44]. Two dissolutions were prepared to obtain the SiO_2 sol: (1) TEOS was added to ethanol in a 1:4 molar ratio of TEOS:ethanol, and (2) HCl was added to deionized water in a 530:1 molar ratio of H_2O:HCl and stirred for one hour. Then, the solutions were mixed and stirred for 21 h [45]. The Lu_2O_3 and SiO_2 solutions were mixed in a 1:1 molar ratio and stirred for 2 h to obtain the Lu_2SiO_5 sol [46]. Glymo was

added as a cross-linking agent to all samples in a molar ratio of 1.3 of Glymo:Lu_2SiO_5. The samples were named LSG, corresponding to the pure sample, LSG:Eu (lutetium silicate doped with Eu^{3+}, 5% mol) and LSG:Eu/Yb (lutetium silicate co-doped with Eu^{3+}, 5% mol and Yb^{3+}, 5% mol). A detailed description of the main reactions and the proposed reaction mechanism for the Lu–Si–Glymo complex formation is reported in our previous paper [47].

3.2. Characterization

The crystalline structures were analyzed by X-ray diffraction (XRD) using a powder diffractometer Bruker D8 Advance with Cu target and kα radiation (1.5406 Å), at a step of 0.02° and a θ/2θ equipment configuration in the range of 10 to 70°. The powder morphology was assessed using a Quanta FEG 250 scanning electron microscope operated at 15 kV. EPR spectroscopy was performed on a Bruker ELEXSYS II E 500 spectrometer with X-band (~9.5 GHz) at 77 K. Photoluminescence studies were performed on an F-7000 FL spectrophotometer (Hitachi High-Technologies Corporation, Tokyo, Japan).

4. Conclusions

Lutetium oxyorthosilicate (Lu_2SiO_5) type B and lutetium pyrosilicate ($Lu_2Si_2O_7$) type B powders were obtained by the Sol–Gel method and calcined at 1100 °C. The addition of Glymo modified the crystalline structure and morphology to form $Lu_2Si_2O_7$, and the incorporation of Eu^{3+} and Yb^{3+} ions was confirmed by XRD. Oxygen vacancies were identified in all the samples besides the F^+ center for LSG:Eu. The formation of defects, like oxygen vacancies, was confirmed in the lutetium silicate systems by photoluminescence studies showing emission signals between 500 and 550 nm. These results provide the basis for the development of luminescent materials in the study of crystalline defects by EPR spectroscopy and their relationship with luminescent properties.

Author Contributions: Conceptualization, A.L.-M. and M.G.-H.; methodology, A.D.C.-M.; validation, D.R.-R. and S.N.A.-A.; formal analysis, S.N.A.-A.; investigation, A.D.C.-M.; resources, A.L.-M., D.R.-R. and M.G.-H.; writing—original draft preparation, A.D.C.-M. and A.L.-M.; writing—review and editing, D.R.-R., S.N.A.-A. and M.G.-H.; visualization, A.D.C.-M. and S.N.A.-A.; supervision, D.R.-R. and A.L.-M. All authors have read and agreed to the published version of the manuscript.

Funding: This work was supported in part by SECIHTI through the Ph.D. Fellowship with CVU:1009053. The authors acknowledge IPN and SIP-IPN for 20241383, 20251105 and 20253472 projects for supporting this work.

Institutional Review Board Statement: Not applicable.

Informed Consent Statement: Not applicable.

Data Availability Statement: The original contributions presented in this study are included in the article. Further inquiries can be directed to the corresponding author.

Acknowledgments: The experimental support of CNMN-IPN in the execution of the presented work is also acknowledged.

Conflicts of Interest: The authors declare no conflicts of interest.

References

1. Zhu, X.; Pu, Y.; Pu, X.; Xie, X.; Liu, M.; Li, Q. Correlation of oxygen defects variations to band gap changes in luminescence properties of $SrZnO_2$:0.0_2 Eu^{3+} phosphors. *Mater. Lett.* **2019**, *254*, 21–23. [CrossRef]
2. Das, K.; Sharma, S.N.; Kumar, M.; De, S.K. Morphology dependent luminescence properties of Co doped TiO_2 nanostructures. *J. Phys. Chem. C* **2009**, *113*, 14783–14792. [CrossRef]
3. Gajović, A.; Tomašić, N.; Djerdj, I.; Su, D.S.; Furić, K. Influence of mechanochemical processing to luminescence properties in Y_2O_3 powder. *J. Alloys Compd.* **2008**, *456*, 313–319. [CrossRef]

4. Gu, X.; Luo, Y.; Li, Q.; Wang, R.; Fu, S.; Lv, X.; He, Q.; Zhang, Y.; Yan, Q.; Xu, X.; et al. First-Principle Insight Into the Effects of Oxygen Vacancies on the Electronic, Photocatalytic, and Optical Properties of Monoclinic $BiVO_4$(001). *Front. Chem.* **2020**, *8*, 601983. [CrossRef] [PubMed]
5. Cooke, D.W.; Blair, M.W.; Smith, J.F.; Bennett, B.L.; Jacobsohn, L.G.; McKigney, E.A.; Muenchausen, R.E. EPR and luminescence of F+ centers in bulk and nanophosphor oxyorthosilicates. *IEEE Trans. Nucl. Sci.* **2008**, *55*, 1118–1122. [CrossRef]
6. Ji, W.; Lee, M.-H.; Hao, L.; Xu, X.; Agathopoulos, S.; Zheng, D.; Fang, C. Role of oxygen vacancy on the photoluminescence of $BaMgSiO_4$:Eu phosphors: Experimental and theoretical analysis. *Inorg. Chem.* **2015**, *54*, 1556–1562. [CrossRef]
7. Jia, L.; Zhu, J.; Teng, Y.; Gu, M. Effect of Li doping on the O vacancies in Lu_2SiO_5:Ce phosphors. *Mater. Lett.* **2018**, *228*, 372–374. [CrossRef]
8. Jia, Y.; Miglio, A.; Gonze, X.; Mikami, M. Ab-initio study of oxygen vacancy stability in bulk and Cerium-doped lutetium oxyorthosilicate. *J. Lumin.* **2018**, *204*, 499–505. [CrossRef]
9. Chewpraditkul, W.; Moszynski, M. Scintillation properties of $Lu_3Al_5O_{12}$, Lu_2SiO_5 and $LaBr_3$ crystals activated with cerium. *Phys. Procedia* **2011**, *22*, 218–226. [CrossRef]
10. Xie, J.; Shi, Y.; Fan, L.; Xu, Z. Microstructure and luminescent properties of Ce:Lu_2SiO_5 ceramic scintillator by spark plasma sintering. *Opt. Mater.* **2013**, *35*, 744–747. [CrossRef]
11. Fan, L.; Shi, Y.; Xu, J.; Xie, J.; Lei, F. Consolidation of translucent Ce^{3+}-doped Lu_2SiO_5 scintillation ceramics by pressureless sintering. *J. Mater. Res.* **2014**, *29*, 2252–2259. [CrossRef]
12. Mansuy, C.; Dujardin, C.; Mahiou, R.; Nedelec, J.M. Characterization and scintillation properties of sol-gel derived Lu_2SiO_5:Ln^{3+} (Ln = Ce, Eu and Tb) powders. *Opt. Mater.* **2009**, *31*, 1334–1336. [CrossRef]
13. Li, D.Z.; Xu, X.D.; Zhou, D.H.; Xia, C.T.; Wu, F.; Xu, J.; Cong, Z.H.; Zhang, J.; Tang, D.Y. Crystal growth, optical properties, and continuous-wave laser operation of Nd^{3+}-doped Lu_2SiO_5 crystal. *Laser Phys. Lett.* **2011**, *8*, 32–37. [CrossRef]
14. Jiang, Y.; Huang, X.; Hu, S.; Zhao, W.; Wang, J.; Ma, D.; Zhong, J. Preparation and luminescence properties of Ce^{3+}/Sm^{3+} codoped A-Lu_2SiO_5@SiO_2 core-shell nanospheres. *Opt. Mater. Express* **2023**, *13*, 3087. [CrossRef]
15. Liebau, F. *Structural Chemistry of Silicates*; Springer: Berlin/Heidelberg, Germany, 1985. [CrossRef]
16. Kitaura, M.; Tanaka, S.; Itoh, M. Optical properties and electronic structure of Lu_2SiO_5 crystals doped with cerium ions: Thermally-activated energy transfer from host to activator. *J. Lumin.* **2015**, *158*, 226–230. [CrossRef]
17. Mansuy, C.; Leroux, F.; Mahiou, R.; Nedelec, J.M. Preferential site substitution in sol-gel derived Eu^{3+} doped Lu_2SiO_5: A combined study by X-ray absorption and luminescence spectroscopies. *J. Mater. Chem.* **2005**, *15*, 4129–4135. [CrossRef]
18. Bishnoi, A.; Kumar, S.; Joshi, N. *Wide-Angle X-Ray Diffraction (WXRD)*; Elsevier Inc.: Amsterdam, The Netherlands, 2017. [CrossRef]
19. de Jesús Morales-Ramírez, Á.; García-Hernandez, M.; Carrera-Jota, M.L.; Garnica-Chávez, P.; González-Penguelly, B.; Garrido-Hernández, A. Photoluminescence properties of $Lu_2Si_2O_7$: Eu^{3+} sol-gel thin films obtained using GLYMO as a silicon source. *Ceram. Int.* **2023**, *49*, 38165–38173. [CrossRef]
20. Nemeth, S.; Liu, Y.C. Mechanical properties of hybrid sol-gel derived films as a function of composition and thermal treatment. *Thin Solid. Film.* **2009**, *517*, 4888–4891. [CrossRef]
21. Atran, A.A.; Algethami, J.S.; Hegazy, H.H.; Hamdy, M.S. Improving the photoluminescence of CeO_2 nanoparticles via creating oxygen vacancies in the crystal lattice. *Optik* **2024**, *308*, 171818. [CrossRef]
22. Choudhury, B.; Choudhury, A. Ce^{3+} and oxygen vacancy mediated tuning of structural and optical properties of CeO_2 nanoparticles. *Mater. Chem. Phys.* **2012**, *131*, 666–671. [CrossRef]
23. Kuriyan, N.S.; Sabeena, M. Luminescence studies of Eu^{3+} doped calcium magnesium silicate phosphor prepared at different annealing temperatures for fine color tunability. *J. Lumin.* **2022**, *249*, 119038. [CrossRef]
24. McPeak, J.E.; Eaton, S.S.; Eaton, G.R. Electron paramagnetic resonance of lanthanides. *Methods Enzymol.* **2021**, *651*, 63–101. [CrossRef]
25. Patel, D.K.; Rajeswari, B.; Sudarsan, V.; Vatsa, R.K.; Kadam, R.M.; Kulshreshtha, S.K. Structural, luminescence and EPR studies on $SrSnO_3$ nanorods doped with europium ions. *Dalton Trans.* **2012**, *41*, 12023–12030. [CrossRef]
26. Vasyukov, V.N.; Chabanenko, V.V. Manifestation of noncentrality in the EPR spectrum of Fe^{3+} in polycrystalline substances. *Low. Temp. Phys.* **2004**, *30*, 956–960. [CrossRef]
27. Jain, A.; Ong, S.P.; Hautier, G.; Chen, W.; Richards, W.D.; Dacek, S.; Cholia, S.; Gunter, D.; Skinner, D.; Ceder, G.; et al. Commentary: The materials project: A materials genome approach to accelerating materials innovation. *Am. Inst. Phys. Inc.* **2013**, *8207*, 118. [CrossRef]
28. Kappers, L.A.; Gilliam, O.R.; Evans, S.M.; Halliburton, L.E.; Giles, N.C. EPR and optical study of oxygen and zinc vacancies in electron-irradiated ZnO. *Nucl. Instrum. Methods Phys. Res. B* **2008**, *266*, 2953–2957. [CrossRef]
29. Rodríguez-Aranda, M.C.; Calderón-Piñar, F.; Hernández-Landaverde, M.A.; Heiras, J.; Zamorano-Ulloa, R.; Ramírez-Rosales, D.; Yáñez-Limón, J.M. Photoluminescence of sol-gel synthesized PZT powders. *J. Lumin.* **2016**, *179*, 280–286. [CrossRef]

30. Singh, P.; Yadav, R.S.; Rai, S.B. Enhanced photoluminescence in a Eu^{3+} doped $CaTiO_3$ perovskite phosphor via incorporation of alkali ions for white LEDs. *J. Phys. Chem. Solids* **2021**, *151*, 109916. [CrossRef]
31. Zhao, H.; Wang, H.; Zhao, J.; Zhang, Y.; Li, K.; Yu, J. Effect of oxygen vacancy on photoluminescence properties of Dy^{3+} doped $K_2BaCa(PO_4)_2$ phosphor and remote luminescence multi-layer for white light. *J. Alloys Compd.* **2023**, *958*, 170505. [CrossRef]
32. Zhou, J.; Zhong, J.; Guo, J.; Liang, H.; Su, Q.; Tang, Q.; Tao, Y.; Moretti, F.; Lebbou, K.; Dujardin, C. The Influence of Oxygen Vacancies on Luminescence Properties of $Na_3LuSi_3O_9$: Ce^{3+}. *J. Phys. Chem. C* **2016**, *120*, 18741–18747. [CrossRef]
33. Kaftelen, H.; Ocakoglu, K.; Thomann, R.; Tu, S.; Weber, S.; Erdem, E. EPR and photoluminescence spectroscopy studies on the defect structure of ZnO nanocrystals. *Phys. Rev. B Condens. Matter Mater. Phys.* **2012**, *86*, 014113. [CrossRef]
34. Kumar, U.; Upadhyay, S.; Alvi, P.A. Study of reaction mechanism, structural, optical and oxygen vacancy-controlled luminescence properties of Eu-modified Sr_2SnO_4 Ruddlesden popper oxide. *Phys. B Condens. Matter* **2021**, *604*, 412708. [CrossRef]
35. Luo, L.; Liu, R.; Liu, Y.; Zhuang, W.; Li, Y.; Gao, T. Effects of oxygen vacancies on luminescent properties of phosphor $Sr_4Al_{14}O_{25}$:Mn^{4+} co-doping with alkali metal ion. *Inorg. Chem. Commun.* **2020**, *118*, 107972. [CrossRef]
36. Manju; Jain, M.; Madas, S.; Vashishtha, P.; Rajput, P.; Gupta, G.; Kahaly, M.U.; Özdoğan, K.; Vij, A.; Thakur, A. Oxygen vacancies induced photoluminescence in $SrZnO_2$ nanophosphors probed by theoretical and experimental analysis. *Sci. Rep.* **2020**, *10*, 17364. [CrossRef]
37. Altunal, V.; Guckan, V.; Yegingil, Z. Effects of oxygen vacancies on luminescence characteristics of BeO ceramics. *J. Alloys Compd.* **2023**, *938*, 168670. [CrossRef]
38. Ferrier, A.; Tumino, B.; Goldner, P. Variations in the oscillator strength of the $^7F_0 \rightarrow {}^5D_0$ transition in Eu^{3+}: Y_2SiO_5 single crystals. *J. Lumin.* **2016**, *170*, 406–410. [CrossRef]
39. Xie, H.; Xu, L.; Qin, L.; Huang, Y.; Wei, D.; Kim, S.I.; Seo, H.J. Orange-emitting $Ba_4R_2ZrWO_{12}$:Eu^{3+} (R=La, Gd, Y) with the strongest $^5D_0 \rightarrow {}^7F_0$ transition. *Mater. Lett.* **2014**, *115*, 18–20. [CrossRef]
40. Souza, A.S.; Couto Dos Santos, M.A. The J-mixing effect in Ln^{3+} ions crystal field levels. *Chem. Phys. Lett.* **2012**, *521*, 138–141. [CrossRef]
41. Binnemans, K. Interpretation of europium(III) spectra. *Coord. Chem. Rev.* **2015**, *295*, 1–45. [CrossRef]
42. Fan, L.; Lin, D.; Zhang, X.; Shi, Y.; Zhang, J.; Xie, J.; Lei, F.; Zhang, L. Local structures of Lu atoms in a core-shell approach for synthesis of Lu_2SiO_5 phase. *Chem. Phys. Lett.* **2016**, *644*, 41–44. [CrossRef]
43. Lu, Q.; Liu, Q.; Wei, Q.; Liu, G.; Zhuang, J. Preparation and characterization of Lu_2SiO_5:Ce^{3+} luminescent ceramic fibers via electrospinning. *Ceram. Int.* **2013**, *39*, 8159–8164. [CrossRef]
44. Carrera-Jota, M.L.; García-Hernández, M.; García-Murillo, A.; Carrillo-Romo, F.J.; Rivera-Becerril, E.; Morales-Ramírez, A.J.; Desirena-Enriquez, H.; de la Rosa-Cruz, E. Synthesis of Lu_2O_3:Eu^{3+} Luminescent Ceramic Powder Embedded in SiO_2 Matrix. *Mater. Trans.* **2014**, *55*, 1867–1871. [CrossRef]
45. Carrera-Jota, M.L.; García-Murillo, A.; Carrillo-Romo, F.; García-Hernández, M.; Morales-Ramírez, A.D.J.; Velumani, S.; de la Rosa-Cruz, E.; Kassiba, A. Lu2O3: Eu3+ glass ceramic films: Synthesis, structural and spectroscopic studies. *Mater. Res. Bull.* **2014**, *51*, 418–425. [CrossRef]
46. Shin, D.Y.; Cao, G.; Kim, K.N. Prepration and photoluminescence properties of Ce doped lutetium silicate nanopowders by sol-gel method. *Curr. Appl. Phys.* **2011**, *11*, S309–S312. [CrossRef]
47. Cancino-Moreno, A.D.; López-Marure, A.; Luna-Domínguez, J.H.; Morales-Ramírez, A.D.J.; Ortega-Avilés, M.; Álvarez-Chávez, J.A.; García-Hernández, M. Effect of Glymo on the Morphological and Optical Properties of Eu^{3+}-Doped Lu_2SiO_5 Films. *Coatings* **2023**, *13*, 915. [CrossRef]

Disclaimer/Publisher's Note: The statements, opinions and data contained in all publications are solely those of the individual author(s) and contributor(s) and not of MDPI and/or the editor(s). MDPI and/or the editor(s) disclaim responsibility for any injury to people or property resulting from any ideas, methods, instructions or products referred to in the content.